

Search for the lightest scalar top quark in events with two leptons in $p\bar{p}$ collisions at $\sqrt{s} = 1.96$ TeV

V.M. Abazov³⁵, B. Abbott⁷⁵, M. Abolins⁶⁵, B.S. Acharya²⁸, M. Adams⁵¹, T. Adams⁴⁹, E. Aguilo⁵, S.H. Ahn³⁰, M. Ahsan⁵⁹, G.D. Alexeev³⁵, G. Alkhazov³⁹, A. Alton^{64,a}, G. Alverson⁶³, G.A. Alves², M. Anastasoie³⁴, L.S. Ancu³⁴, T. Andeen⁵³, S. Anderson⁴⁵, B. Andrieu¹⁶, M.S. Anzels⁵³, Y. Arnoud¹³, M. Arov⁶⁰, M. Arthaud¹⁷, A. Askew⁴⁹, B. Åsman⁴⁰, A.C.S. Assis Jesus³, O. Atramentov⁴⁹, C. Autermann²⁰, C. Avila⁷, C. Ay²³, F. Badaud¹², A. Baden⁶¹, L. Bagby⁵², B. Baldin⁵⁰, D.V. Bandurin⁵⁹, S. Banerjee²⁸, P. Banerjee²⁸, E. Barberis⁶³, A.-F. Barfuss¹⁴, P. Bargassa⁸⁰, P. Baringer⁵⁸, J. Barreto², J.F. Bartlett⁵⁰, U. Bassler¹⁶, D. Bauer⁴³, S. Beale⁵, A. Bean⁵⁸, M. Begalli³, M. Biegel⁷¹, C. Belanger-Champagne⁴⁰, L. Bellantoni⁵⁰, A. Bellavance⁵⁰, J.A. Benitez⁶⁵, S.B. Beri²⁶, G. Bernardi¹⁶, R. Bernhard²², L. Berntzon¹⁴, I. Bertram⁴², M. Besançon¹⁷, R. Beuselinck⁴³, V.A. Bezzubov³⁸, P.C. Bhat⁵⁰, V. Bhatnagar²⁶, C. Biscarat¹⁹, G. Blazey⁵², F. Blekman⁴³, S. Blessing⁴⁹, D. Bloch¹⁸, K. Bloom⁶⁷, A. Boehnlein⁵⁰, D. Boline⁶², T.A. Bolton⁵⁹, G. Borissov⁴², K. Bos³³, T. Bose⁷⁷, A. Brandt⁷⁸, R. Brock⁶⁵, G. Brooijmans⁷⁰, A. Bross⁵⁰, D. Brown⁷⁸, N.J. Buchanan⁴⁹, D. Buchholz⁵³, M. Buehler⁸¹, V. Buescher²¹, S. Burdin^{42,b}, S. Burke⁴⁵, T.H. Burnett⁸², C.P. Buszello⁴³, J.M. Butler⁶², P. Calfayan²⁴, S. Calvet¹⁴, J. Cammin⁷¹, S. Caron³³, W. Carvalho³, B.C.K. Casey⁷⁷, N.M. Cason⁵⁵, H. Castilla-Valdez³², S. Chakrabarti¹⁷, D. Chakraborty⁵², K.M. Chan⁵⁵, K. Chan⁵, A. Chandra⁴⁸, F. Charles^{18,‡}, E. Cheu⁴⁵, F. Chevallier¹³, D.K. Cho⁶², S. Choi³¹, B. Choudhary²⁷, L. Christofek⁷⁷, T. Christoudias^{43,†}, S. Cihangir⁵⁰, D. Claes⁶⁷, B. Clément¹⁸, Y. Coadou⁵, M. Cooke⁸⁰, W.E. Cooper⁵⁰, M. Corcoran⁸⁰, F. Couderc¹⁷, M.-C. Cousinou¹⁴, S. Crépe-Renaudin¹³, D. Cutts⁷⁷, M. Cwiok²⁹, H. da Motta², A. Das⁶², G. Davies⁴³, K. De⁷⁸, S.J. de Jong³⁴, P. de Jong³³, E. De La Cruz-Burelo⁶⁴, C. De Oliveira Martins³, J.D. Degenhardt⁶⁴, F. Déliot¹⁷, M. Demarteau⁵⁰, R. Demina⁷¹, D. Denisov⁵⁰, S.P. Denisov³⁸, S. Desai⁵⁰, H.T. Diehl⁵⁰, M. Diesburg⁵⁰, A. Dominguez⁶⁷, H. Dong⁷², L.V. Dudko³⁷, L. Duflot¹⁵, S.R. Dugad²⁸, D. Duggan⁴⁹, A. Duperrin¹⁴, J. Dyer⁶⁵, A. Dyshkant⁵², M. Eads⁶⁷, D. Edmunds⁶⁵, J. Ellison⁴⁸, V.D. Elvira⁵⁰, Y. Enari⁷⁷, S. Eno⁶¹, P. Ermolov³⁷, H. Evans⁵⁴, A. Evdokimov⁷³, V.N. Evdokimov³⁸, A.V. Ferapontov⁵⁹, T. Ferbel⁷¹, F. Fiedler²⁴, F. Filthaut³⁴, W. Fisher⁵⁰, H.E. Fisk⁵⁰, M. Ford⁴⁴, M. Fortner⁵², H. Fox²², S. Fu⁵⁰, S. Fuess⁵⁰, T. Gadfort⁸², C.F. Galea³⁴, E. Gallas⁵⁰, E. Galyaev⁵⁵, C. Garcia⁷¹, A. Garcia-Bellido⁸², V. Gavrilov³⁶, P. Gay¹², W. Geist¹⁸, D. Gelé¹⁸, C.E. Gerber⁵¹, Y. Gershtein⁴⁹, D. Gillberg⁵, G. Ginter⁷¹, N. Gollub⁴⁰, B. Gómez⁷, A. Goussiou⁵⁵, P.D. Grannis⁷², H. Greenlee⁵⁰, Z.D. Greenwood⁶⁰, E.M. Gregores⁴, G. Grenier¹⁹, Ph. Gris¹², J.-F. Grivaz¹⁵, A. Grohsjean²⁴, S. Grünendahl⁵⁰, M.W. Grünwald²⁹, J. Guo⁷², F. Guo⁷², P. Gutierrez⁷⁵, G. Gutierrez⁵⁰, A. Haas⁷⁰, N.J. Hadley⁶¹, P. Haefner²⁴, S. Hagopian⁴⁹, J. Haley⁶⁸, I. Hall⁶⁵, R.E. Hall⁴⁷, L. Han⁶, K. Hanagaki⁵⁰, P. Hansson⁴⁰, K. Harder⁴⁴, A. Harel⁷¹, R. Harrington⁶³, J.M. Hauptman⁵⁷, R. Hauser⁶⁵, J. Hays⁴³, T. Hebbeker²⁰, D. Hedin⁵², J.G. Hegeman³³, J.M. Heinmiller⁵¹, A.P. Heinson⁴⁸, U. Heintz⁶², C. Hensel⁵⁸, K. Herner⁷², G. Hesketh⁶³, M.D. Hildreth⁵⁵, R. Hirosky⁸¹, J.D. Hobbs⁷², B. Hoeneisen¹¹, H. Hoeth²⁵, M. Hohlfeld²¹, S.J. Hong³⁰, R. Hooper⁷⁷, S. Hossain⁷⁵, P. Houben³³, Y. Hu⁷², Z. Hubacek⁹, V. Hynek⁸, I. Iashvili⁶⁹, R. Illingworth⁵⁰, A.S. Ito⁵⁰, S. Jabeen⁶², M. Jaffré¹⁵, S. Jain⁷⁵, K. Jakobs²², C. Jarvis⁶¹, R. Jesik⁴³, K. Johns⁴⁵, C. Johnson⁷⁰, M. Johnson⁵⁰, A. Jonckheere⁵⁰, P. Jonsson⁴³, A. Juste⁵⁰, D. Käfer²⁰, S. Kahn⁷³, E. Kajfasz¹⁴, A.M. Kalinin³⁵, J.R. Kalk⁶⁵, J.M. Kalk⁶⁰, S. Kappler²⁰, D. Karmanov³⁷, J. Kasper⁶², P. Kasper⁵⁰, I. Katsanos⁷⁰, D. Kau⁴⁹, R. Kaur²⁶, V. Kaushik⁷⁸, R. Kehoe⁷⁹, S. Kermiche¹⁴, N. Khalatyan³⁸, A. Khanov⁷⁶, A. Kharchilava⁶⁹, Y.M. Kharzheev³⁵, D. Khatidze⁷⁰, H. Kim³¹, T.J. Kim³⁰, M.H. Kirby³⁴, M. Kirsch²⁰, B. Klima⁵⁰, J.M. Kohli²⁶, J.-P. Konrath²², M. Kopal⁷⁵, V.M. Korablev³⁸, A.V. Kozelov³⁸, D. Krop⁵⁴, A. Kryemadhi⁸¹, T. Kuhl²³, A. Kumar⁶⁹, S. Kunori⁶¹, A. Kupco¹⁰, T. Kurča¹⁹, J. Kvita⁸, F. Lacroix¹², D. Lam⁵⁵, S. Lammers⁷⁰, G. Landsberg⁷⁷, J. Lazoflores⁴⁹, P. Lebrun¹⁹, W.M. Lee⁵⁰, A. Leftat³⁷, F. Lehner⁴¹, J. Lellouch¹⁶, J. Leveque⁴⁵, P. Lewis⁴³, J. Li⁷⁸, Q.Z. Li⁵⁰, L. Li⁴⁸, S.M. Lietti⁴, J.G.R. Lima⁵², D. Lincoln⁵⁰, J. Linnemann⁶⁵, V.V. Lipaev³⁸, R. Lipton⁵⁰, Y. Liu^{6,†}, Z. Liu⁵, L. Lobo⁴³, A. Lobodenko³⁹, M. Lokajicek¹⁰, A. Lounis¹⁸, P. Love⁴², H.J. Lubatti⁸², A.L. Lyon⁵⁰, A.K.A. Maciel², D. Mackin⁸⁰, R.J. Madaras⁴⁶, P. Mättig²⁵, C. Magass²⁰, A. Magerkurth⁶⁴, N. Makovec¹⁵, P.K. Mal⁵⁵, H.B. Malbouisson³, S. Malik⁶⁷, V.L. Malyshev³⁵, H.S. Mao⁵⁰, Y. Maravin⁵⁹, B. Martin¹³, R. McCarthy⁷², A. Melnitchouk⁶⁶, A. Mendes¹⁴, L. Mendoza⁷, P.G. Mercadante⁴, M. Merkin³⁷, K.W. Merritt⁵⁰, J. Meyer²¹, A. Meyer²⁰, M. Michaut¹⁷, T. Millet¹⁹, J. Mitrevski⁷⁰, J. Molina³, R.K. Mommsen⁴⁴, N.K. Mondal²⁸, R.W. Moore⁵, T. Moulík⁵⁸, G.S. Muanza¹⁹, M. Mulders⁵⁰, M. Mulhearn⁷⁰, O. Mundal²¹, L. Mundim³, E. Nagy¹⁴, M. Naimuddin⁵⁰,

M. Narain⁷⁷, N.A. Naumann³⁴, H.A. Neal⁶⁴, J.P. Negret⁷, P. Neustroev³⁹, H. Nilsen²², A. Nomerotski⁵⁰, S.F. Novaes⁴, T. Nunnemann²⁴, V. O'Dell⁵⁰, D.C. O'Neil⁵, G. Obrant³⁹, C. Ochando¹⁵, D. Onoprienko⁵⁹, N. Oshima⁵⁰, J. Osta⁵⁵, R. Otec⁹, G.J. Otero y Garzón⁵¹, M. Owen⁴⁴, P. Padley⁸⁰, M. Pangilinan⁷⁷, N. Parashar⁵⁶, S.-J. Park⁷¹, S.K. Park³⁰, J. Parsons⁷⁰, R. Partridge⁷⁷, N. Parua⁵⁴, A. Patwa⁷³, G. Pawloski⁸⁰, B. Penning²², K. Peters⁴⁴, Y. Peters²⁵, P. Pétrouff¹⁵, M. Petteni⁴³, R. Piegaia¹, J. Piper⁶⁵, M.-A. Pleier²¹, P.L.M. Podesta-Lerma^{32,d}, V.M. Podstavkov⁵⁰, Y. Pogorelov⁵⁵, M.-E. Pol², P. Polozov³⁶, A. Pompo[~], B.G. Pope⁶⁵, A.V. Popov³⁸, C. Potter⁵, W.L. Prado da Silva³, H.B. Prosper⁴⁹, S. Protopopescu⁷³, J. Qian⁶⁴, A. Quadt^{21,e}, B. Quinn⁶⁶, A. Rakitine⁴², M.S. Rangel², K. Ranjan²⁷, P.N. Ratoff⁴², P. Renkel⁷⁹, S. Reucroft⁶³, P. Rich⁴⁴, M. Rijssenbeek⁷², I. Ripp-Baudot¹⁸, F. Rizatdinova⁷⁶, S. Robinson⁴³, R.F. Rodrigues³, C. Royon¹⁷, P. Rubinov⁵⁰, R. Ruchti⁵⁵, G. Safronov³⁶, G. Sajot¹³, A. Sánchez-Hernández³², M.P. Sanders¹⁶, A. Santoro³, G. Savage⁵⁰, L. Sawyer⁶⁰, T. Scanlon⁴³, D. Schaile²⁴, R.D. Schamberger⁷², Y. Scheglov³⁹, H. Schellman⁵³, P. Schieferdecker²⁴, T. Schliephake²⁵, C. Schwanenberger⁴⁴, A. Schwartzman⁶⁸, R. Schwienhorst⁶⁵, J. Sekaric⁴⁹, S. Sengupta⁴⁹, H. Severini⁷⁵, E. Shabalina⁵¹, M. Shamim⁵⁹, V. Shary¹⁷, A.A. Shchukin³⁸, R.K. Shivpuri²⁷, D. Shpakov⁵⁰, V. Siccari¹⁸, V. Simak⁹, V. Sirotenko⁵⁰, P. Skubic⁷⁵, P. Slattery⁷¹, D. Smirnov⁵⁵, J. Snow⁷⁴, G.R. Snow⁶⁷, S. Snyder⁷³, S. Söldner-Rembold⁴⁴, L. Sonnenschein¹⁶, A. Sopczak⁴², M. Sosebee⁷⁸, K. Soustruznik⁸, M. Souza², B. Spurlock⁷⁸, J. Stark¹³, J. Steele⁶⁰, V. Stolin³⁶, A. Stone⁵¹, D.A. Stoyanova³⁸, J. Strandberg⁶⁴, S. Strandberg⁴⁰, M.A. Strang⁶⁹, M. Strauss⁷⁵, E. Strauss⁷², R. Ströhmer²⁴, D. Strom⁵³, L. Stutte⁵⁰, S. Sumowidagdo⁴⁹, P. Svoisky⁵⁵, A. Sznajder³, M. Talby¹⁴, P. Tamburello⁴⁵, A. Tanasijczuk¹, W. Taylor⁵, P. Telford⁴⁴, J. Temple⁴⁵, B. Tiller²⁴, F. Tissandier¹², M. Titov¹⁷, V.V. Tokmenin³⁵, T. Toole⁶¹, I. Torchiani²², T. Trefzger²³, D. Tsybychev⁷², B. Tuchming¹⁷, C. Tully⁶⁸, P.M. Tuts⁷⁰, R. Unalan⁶⁵, S. Uvarov³⁹, L. Uvarov³⁹, S. Uzunyan⁵², B. Vachon⁵, P.J. van den Berg³³, B. van Eijk³³, R. Van Kooten⁵⁴, W.M. van Leeuwen³³, N. Varelas⁵¹, E.W. Varnes⁴⁵, I.A. Vasilyev³⁸, M. Vaupel²⁵, P. Verdier¹⁹, L.S. Vertogradov³⁵, M. Verzocchi⁵⁰, F. Villeneuve-Segui⁴³, P. Vint⁴³, P. Vokac⁹, E. Von Toerne⁵⁹, M. Voutilainen^{67,f}, M. Vreeswijk³³, R. Wagner⁶⁸, H.D. Wahl⁴⁹, L. Wang⁶¹, M.H.L.S Wang⁵⁰, J. Warchol⁵⁵, G. Watts⁸², M. Wayne⁵⁵, M. Weber⁵⁰, G. Weber²³, A. Wenger^{22,g}, N. Wermes²¹, M. Wetstein⁶¹, A. White⁷⁸, D. Wicke²⁵, G.W. Wilson⁵⁸, S.J. Wimpenny⁴⁸, M. Wobisch⁶⁰, D.R. Wood⁶³, T.R. Wyatt⁴⁴, Y. Xie⁷⁷, S. Yacoub⁵³, R. Yamada⁵⁰, M. Yan⁶¹, T. Yasuda⁵⁰, Y.A. Yatsunenko³⁵, K. Yip⁷³, H.D. Yoo⁷⁷, S.W. Youn⁵³, J. Yu⁷⁸, A. Zatserklyaniy⁵², C. Zeitnitz²⁵, D. Zhang⁵⁰, T. Zhao⁸², B. Zhou⁶⁴, J. Zhu⁷², M. Zielinski⁷¹, D. Zieminska⁵⁴, A. Zieminski⁵⁴, L. Zivkovic⁷⁰, V. Zutshi⁵², and E.G. Zverev³⁷

(The DØ Collaboration)

¹Universidad de Buenos Aires, Buenos Aires, Argentina

²LAFEX, Centro Brasileiro de Pesquisas Físicas, Rio de Janeiro, Brazil

³Universidade do Estado do Rio de Janeiro, Rio de Janeiro, Brazil

⁴Instituto de Física Teórica, Universidade Estadual Paulista, São Paulo, Brazil

⁵University of Alberta, Edmonton, Alberta, Canada,

Simon Fraser University, Burnaby, British Columbia,

Canada, York University, Toronto, Ontario, Canada,

and McGill University, Montreal, Quebec, Canada

⁶University of Science and Technology of China, Hefei, People's Republic of China

⁷Universidad de los Andes, Bogotá, Colombia

⁸Center for Particle Physics, Charles University, Prague, Czech Republic

⁹Czech Technical University, Prague, Czech Republic

¹⁰Center for Particle Physics, Institute of Physics,

Academy of Sciences of the Czech Republic, Prague, Czech Republic

¹¹Universidad San Francisco de Quito, Quito, Ecuador

¹²Laboratoire de Physique Corpusculaire, IN2P3-CNRS,

Université Blaise Pascal, Clermont-Ferrand, France

¹³Laboratoire de Physique Subatomique et de Cosmologie,

IN2P3-CNRS, Université de Grenoble 1, Grenoble, France

¹⁴CPPM, IN2P3-CNRS, Université de la Méditerranée, Marseille, France

¹⁵Laboratoire de l'Accélérateur Linéaire, IN2P3-CNRS et Université Paris-Sud, Orsay, France

¹⁶LPNHE, IN2P3-CNRS, Universités Paris VI and VII, Paris, France

¹⁷DAPNIA/Service de Physique des Particules, CEA, Saclay, France

¹⁸IPHC, Université Louis Pasteur et Université de Haute Alsace, CNRS, IN2P3, Strasbourg, France

¹⁹IPNL, Université Lyon 1, CNRS/IN2P3, Villeurbanne, France and Université de Lyon, Lyon, France

²⁰III. Physikalisches Institut A, RWTH Aachen, Aachen, Germany

²¹Physikalisches Institut, Universität Bonn, Bonn, Germany

- ²²Physikalisches Institut, Universität Freiburg, Freiburg, Germany
²³Institut für Physik, Universität Mainz, Mainz, Germany
²⁴Ludwig-Maximilians-Universität München, München, Germany
²⁵Fachbereich Physik, University of Wuppertal, Wuppertal, Germany
²⁶Panjab University, Chandigarh, India
²⁷Delhi University, Delhi, India
²⁸Tata Institute of Fundamental Research, Mumbai, India
²⁹University College Dublin, Dublin, Ireland
³⁰Korea Detector Laboratory, Korea University, Seoul, Korea
³¹SungKyunKwan University, Suwon, Korea
³²CINVESTAV, Mexico City, Mexico
³³FOM-Institute NIKHEF and University of Amsterdam/NIKHEF, Amsterdam, The Netherlands
³⁴Radboud University Nijmegen/NIKHEF, Nijmegen, The Netherlands
³⁵Joint Institute for Nuclear Research, Dubna, Russia
³⁶Institute for Theoretical and Experimental Physics, Moscow, Russia
³⁷Moscow State University, Moscow, Russia
³⁸Institute for High Energy Physics, Protvino, Russia
³⁹Petersburg Nuclear Physics Institute, St. Petersburg, Russia
⁴⁰Lund University, Lund, Sweden, Royal Institute of Technology and Stockholm University, Stockholm, Sweden, and Uppsala University, Uppsala, Sweden
⁴¹Physik Institut der Universität Zürich, Zürich, Switzerland
⁴²Lancaster University, Lancaster, United Kingdom
⁴³Imperial College, London, United Kingdom
⁴⁴University of Manchester, Manchester, United Kingdom
⁴⁵University of Arizona, Tucson, Arizona 85721, USA
⁴⁶Lawrence Berkeley National Laboratory and University of California, Berkeley, California 94720, USA
⁴⁷California State University, Fresno, California 93740, USA
⁴⁸University of California, Riverside, California 92521, USA
⁴⁹Florida State University, Tallahassee, Florida 32306, USA
⁵⁰Fermi National Accelerator Laboratory, Batavia, Illinois 60510, USA
⁵¹University of Illinois at Chicago, Chicago, Illinois 60607, USA
⁵²Northern Illinois University, DeKalb, Illinois 60115, USA
⁵³Northwestern University, Evanston, Illinois 60208, USA
⁵⁴Indiana University, Bloomington, Indiana 47405, USA
⁵⁵University of Notre Dame, Notre Dame, Indiana 46556, USA
⁵⁶Purdue University Calumet, Hammond, Indiana 46323, USA
⁵⁷Iowa State University, Ames, Iowa 50011, USA
⁵⁸University of Kansas, Lawrence, Kansas 66045, USA
⁵⁹Kansas State University, Manhattan, Kansas 66506, USA
⁶⁰Louisiana Tech University, Ruston, Louisiana 71272, USA
⁶¹University of Maryland, College Park, Maryland 20742, USA
⁶²Boston University, Boston, Massachusetts 02215, USA
⁶³Northeastern University, Boston, Massachusetts 02115, USA
⁶⁴University of Michigan, Ann Arbor, Michigan 48109, USA
⁶⁵Michigan State University, East Lansing, Michigan 48824, USA
⁶⁶University of Mississippi, University, Mississippi 38677, USA
⁶⁷University of Nebraska, Lincoln, Nebraska 68588, USA
⁶⁸Princeton University, Princeton, New Jersey 08544, USA
⁶⁹State University of New York, Buffalo, New York 14260, USA
⁷⁰Columbia University, New York, New York 10027, USA
⁷¹University of Rochester, Rochester, New York 14627, USA
⁷²State University of New York, Stony Brook, New York 11794, USA
⁷³Brookhaven National Laboratory, Upton, New York 11973, USA
⁷⁴Langston University, Langston, Oklahoma 73050, USA
⁷⁵University of Oklahoma, Norman, Oklahoma 73019, USA
⁷⁶Oklahoma State University, Stillwater, Oklahoma 74078, USA
⁷⁷Brown University, Providence, Rhode Island 02912, USA
⁷⁸University of Texas, Arlington, Texas 76019, USA
⁷⁹Southern Methodist University, Dallas, Texas 75275, USA
⁸⁰Rice University, Houston, Texas 77005, USA
⁸¹University of Virginia, Charlottesville, Virginia 22901, USA and
⁸²University of Washington, Seattle, Washington 98195, USA

(Dated: July 16, 2007)

Data collected by the D0 detector at a $p\bar{p}$ center-of-mass energy of 1.96 TeV at the Fermilab Tevatron Collider have been used to search for pair production of the lightest supersymmetric partner of the top quark decaying into $b\ell\tilde{\nu}$. The search is performed in the $\ell\ell' = e\mu$ and $\mu\mu$ final states. No evidence for this process has been found in data samples of approximately 400 pb^{-1} . The domain in the $[M(\tilde{t}_1), M(\tilde{\nu})]$ plane excluded at the 95% C.L. is substantially extended by this search.

PACS numbers: 14.80.Ly; 12.60.Jv

Supersymmetric theories [1] predict the existence of a scalar partner for each standard model fermion. Because of the large mass of the standard model top quark, the mixing between its chiral supersymmetric partners is the largest among all squarks; therefore the lightest supersymmetric partner of the top quark, \tilde{t}_1 (stop), might be the lightest squark. If the $\tilde{t}_1 \rightarrow b\ell\tilde{\nu}$ decay channel is kinematically accessible, it will be dominant [2] as long as the $\tilde{t}_1 \rightarrow b\tilde{\chi}_1^\pm$ and $\tilde{t}_1 \rightarrow b\tilde{\chi}_1^0$ channels are kinematically closed, where $\tilde{\chi}_1^\pm$ and $\tilde{\chi}_1^0$ are the lightest chargino and neutralino, respectively. In this letter we present a search for stop pair production in $p\bar{p}$ collisions at 1.96 TeV with the D0 detector, where a virtual chargino $\tilde{\chi}^\pm$ decays into a lepton and a sneutrino, and where the $\tilde{\nu}$, considered to be the next lightest supersymmetric particle, decays into a neutrino and the lightest neutralino $\tilde{\chi}_1^0$. We use the minimal supersymmetric standard model as the phenomenological framework for this search. We assume the branching ratio $Br(\tilde{\chi}_1^\pm \rightarrow \ell\tilde{\nu}) = 1$ with equal sharing among all lepton flavors, and we consider only cases where $\ell = e, \mu$. For stop pair production, we consider $b\bar{b} \ell\ell'\nu\bar{\nu}\tilde{\chi}_1^0\tilde{\chi}_1^0$ final states with $\ell\ell' = e^\pm\mu^\mp$ and $\ell\ell' = \mu^+\mu^-$ ($e\mu$ and $\mu\mu$ channels); the signal topology consists of two isolated leptons, missing transverse energy (\cancel{E}_T), and jets. D0 has also searched for scalar top in the charm jet final state [3].

The D0 detector [4] comprises a central tracking system surrounded by a liquid-argon sampling calorimeter and a system of muon detectors. Charged particles are reconstructed using a multi-layer silicon detector and eight double layers of scintillating fibers in a 2 T magnetic field produced by a superconducting solenoid. The calorimeter provides hermetic coverage up to pseudo-rapidities $|\eta| \simeq 4$ in a semi-projective tower geometry with longitudinal segmentation. After passing through the calorimeter, muons are detected in the muon detector comprising three layers of tracking detectors and scintillation counters located inside and outside of 1.8 T iron toroids. Events containing electrons or muons are selected for offline analysis by a trigger system. A set of dilepton triggers is used to tag the presence of electrons and muons based on their energy deposit in the calorimeter, hits in the muon detectors, and tracks in the tracking system.

Three-body decays of the \tilde{t}_1 are simulated using COMPHEP [5] and PYTHIA [6] for generation and hadronization respectively. Standard model background processes are simulated using the PYTHIA and ALPGEN

[7] Monte Carlo (MC) generators. These MC samples are generated using the CTEQ5L [8] parton distribution functions (PDF); they are normalized using next-to-leading order cross sections. All generated events are passed through the full simulation of the detector geometry and response based on GEANT [9]. MC events are then reconstructed and analyzed with the same programs as used for the data.

Muons are reconstructed by finding tracks pointing to hit patterns in the muon system. Non-isolated muons are rejected by requiring the sum of the p_T values of tracks inside a cone with $\Delta\mathcal{R} = \sqrt{(\Delta\phi)^2 + (\Delta\eta)^2} = 0.5$ (where ϕ is the azimuthal angle) around the muon direction, and the calorimeter energy in an annulus of size $0.1 < \Delta\mathcal{R} < 0.4$ around the muon to be less than 4 GeV/c and 4 GeV. Isolated electrons are selected based on their characteristic energy deposition in the calorimeter, their fraction of deposited energy in the electromagnetic portion of the calorimeter and their transverse shower profile inside a cone of radius $\Delta\mathcal{R} = 0.4$ around the direction of the electron; furthermore, it is required that a track points to the energy deposition in the calorimeter and that its momentum and the calorimeter energy are consistent with the same electron energy. Backgrounds from jets and photon conversions are further suppressed by requiring the tracks associated with the muons and electrons to each have at least one hit in the silicon detector. Jets are reconstructed from the energy deposition in calorimeter towers using the Run II cone algorithm [10] with radius $\Delta\mathcal{R}=0.5$; in this search, jets are considered with $p_T > 15 \text{ GeV}/c$. The \cancel{E}_T is defined as the energy imbalance of all calorimeter cells in the plane transverse to the beam direction, and is corrected for the jet energy scale (JES), the electromagnetic energy scale, and reconstructed muons. All efficiencies are measured with data [11].

In both $e\mu$ and $\mu\mu$ channels, the signal points $[M(\tilde{t}_1), M(\tilde{\nu})] = (110, 80) \text{ GeV}/c^2$ and $(145, 50) \text{ GeV}/c^2$, respectively referred as “soft” (point A) and “hard” (point B) signals, have been used to optimize the selection of signals of different kinematics because of different $\Delta m = M(\tilde{t}_1) - M(\tilde{\nu})$. The choice of these points was also motivated by the sensitivity of the D0 search during Run I [12]. The main background processes imitating the signal topology are Z/γ^* , WW , $t\bar{t}$ production, and multijet background. All but the latter are estimated with MC simulation. The multijet background

is estimated from data. Samples dominated by multijet production are obtained by inverting the lepton identification requirements in the $e\mu$ channel, and by requiring same-sign muons in the $\mu\mu$ channel, all other lepton requirements being identical to those of the search sample. These samples are then normalized to the rate of data events with the lepton selection criteria at an early stage of the selection.

For the $e\mu$ channel, the integrated luminosity [13] of the data sample is 428 pb^{-1} . At preselection level, we require the p_T values of the electron and muon (see Figs. 1(a) and (b)) to be greater than 10 and 8 GeV/c , respectively. In this final state, the data are dominated by the multijet and $Z/\gamma^* \rightarrow \tau\tau$ backgrounds. In these processes, poorly reconstructed leptons are correlated with \cancel{E}_T , giving rise to higher event populations at high and low values of the azimuthal angular difference between the leptons and the \cancel{E}_T , a low value of the angular difference for one lepton being correlated with a high value of the other. Taking advantage of a higher background contribution at low values of angular distributions, we require

$$\Delta\phi(\mu, \cancel{E}_T) > 0.4 \text{ rad}, \Delta\phi(e, \cancel{E}_T) > 0.4 \text{ rad} \text{ (Emu 1)}.$$

We require \cancel{E}_T to be greater than 15 GeV to reduce contribution of both the multijet and $Z/\gamma^* \rightarrow \tau\tau$ backgrounds. To reject multijet events in which leptons are associated with a jet, we require the two leptons to be at a distance $\Delta\mathcal{R}$ distance greater than 0.5 from any reconstructed jet. To further reduce the multijet contribution, we require the z component of the origin of the highest transverse momentum muon track to be within four standard deviations σ from the z component of the primary vertex:

$$\begin{aligned} \cancel{E}_T &> 15 \text{ GeV} \\ \Delta\mathcal{R}[(e, \mu), \text{jet}] &> 0.5 \\ |z(\mu) - z(pv)| &< 4\sigma \end{aligned} \quad \text{(Emu 2)}.$$

To reduce the $Z/\gamma^* \rightarrow \tau\tau$ background, we cut on low values of the transverse mass of the muon and \cancel{E}_T ($M_T(\mu, \cancel{E}_T)$, see Fig. 1(c)). To further reduce this background, we make use of the correlation between the angular differences $\Delta\phi(\mu, \cancel{E}_T)$ and $\Delta\phi(e, \cancel{E}_T)$, and require their sum (see Fig. 1(d)) to be greater than 2.9 rad:

$$\begin{aligned} M_T(\mu, \cancel{E}_T) &> 15 \text{ GeV}/c^2 \\ \Delta\phi(\mu, \cancel{E}_T) + \Delta\phi(e, \cancel{E}_T) &> 2.9 \text{ rad} \end{aligned} \quad \text{(Emu 3)}.$$

The contributions of different backgrounds, and the expected numbers of signal and observed data events in the $e\mu$ final state at different selection levels are summarized in Table I. After all selections, the WW (dominating the diboson contribution) and $t\bar{t}$ contributions are the dominant backgrounds. To separate soft signals such as point A from these backgrounds, we consider the variable S_T defined as the scalar sum of the p_T values of the muon,

the electron, and the \cancel{E}_T (see Fig. 1(e)). To separate hard signals such as point B from background contributions, we consider the variable H_T defined as the scalar sum of the p_T values of all jets (see Fig. 1(f)). Rather than cutting on these two variables, the H_T and S_T spectra predicted for signal and background are compared with the observed spectra in twelve $[S_T, H_T]$ bins when extracting limits on the signal cross section, thus allowing a separation of signals of different kinematics from the WW and $t\bar{t}$ backgrounds.

For the $\mu\mu$ channel, the integrated luminosity [13] of the data sample is 395 pb^{-1} . The selection of the signal in this final state is more challenging because of the strongly dominating $Z/\gamma^* \rightarrow \mu\mu$ background. At preselection level, we require the p_T values of the two highest transverse momenta opposite-sign muons to be greater than 8 and 6 GeV/c . While the signal is characterized by the presence of jets originating from the hadronization of b quarks, the $Z/\gamma^* \rightarrow \mu\mu$ background owes the presence of jets to initial state radiation gluons which hadronize into softer jets, resulting in a lower multiplicity of jets; the latter is also valid for soft signals such as point A . To keep sensitivity to soft signals while rejecting substantial background, we require at least one jet:

$$N(\text{jets}) \geq 1 \text{ (Dimu 1)}.$$

To further remove $Z/\gamma^* \rightarrow \mu\mu$ background events, where poorly reconstructed muons correlate with the \cancel{E}_T , we require the \cancel{E}_T to be greater than the contour shown on Fig. 2(a), using a cut parametrized by the following equation:

$$\cancel{E}_T > 20 + |\Delta\phi(\mu_1, \cancel{E}_T) - 1.55|^{9.2} \text{ (Dimu 2)},$$

where μ_1 is the highest transverse momentum muon. To augment the search sensitivity in this channel, we take advantage of the presence of jets originating from the fragmentation of long-lived b quarks in the signal. An algorithm based on the lifetime of hadrons calculates the probability \mathcal{P} for the tracks of a jet to originate from the primary interaction point [14]. This probability is constructed such that its distribution is uniform for light-flavor jets while peaking at zero for heavy-flavor jets which have a vertex significantly displaced from the primary vertex. Considering the highest transverse energy jet, we require

$$\mathcal{P}(\text{jet}) < 1\% \text{ (Dimu 3)}.$$

A cut on the dimuon invariant mass (Fig. 2(b)) in the Z boson peak region only at low \cancel{E}_T (Fig. 2(c)) further suppresses the $Z/\gamma^* \rightarrow \mu\mu$ background while preserving the signal:

$$M(\mu\mu) \notin [75, 120] \text{ GeV}/c^2 \text{ for } \cancel{E}_T < 50 \text{ GeV} \text{ (Dimu 4)}.$$

Table II summarizes the different stages of the signal selection in the $\mu\mu$ channel. The $t\bar{t}$ background dominates after the selection cuts; five H_T bins are considered to separate various signal points from this background.

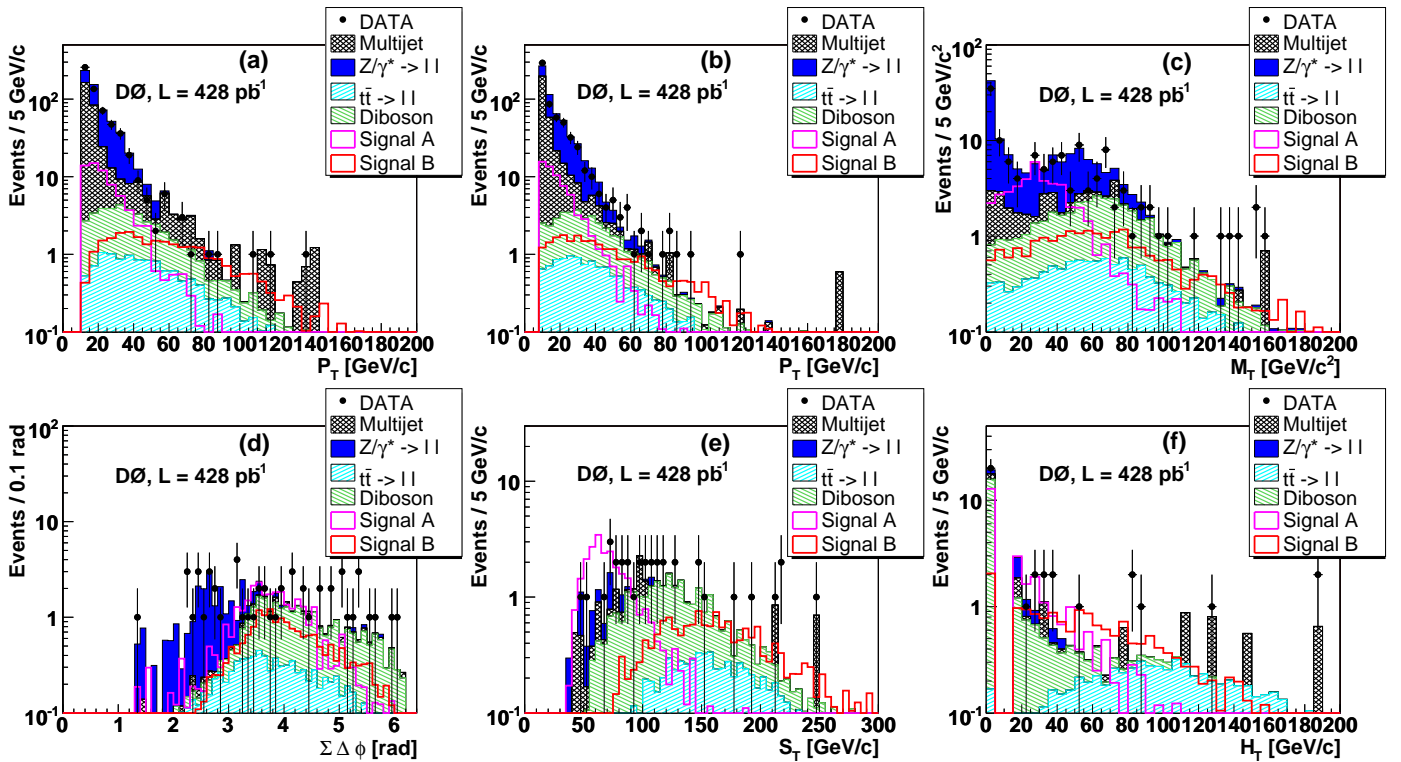


FIG. 1: $e\mu$ channel. Distributions of the p_T of the electron (a) and of the muon (b) after preselection cuts; (c) the transverse mass $M_T(\mu, \cancel{E}_T)$ after preselection cuts and $\cancel{E}_T > 15$ GeV and $\Delta R[(e, \mu), \text{jet}] > 0.5$; (d) the angular sum $\Delta\phi(\mu, \cancel{E}_T) + \Delta\phi(e, \cancel{E}_T)$ after the cut Emu 2; (e) S_T and (f) H_T distributions after the cut Emu 3 (color available online).

TABLE I: $e\mu$ channel. Expected numbers of events in various background and signal channels, and number of observed events in data, at various selection levels. Statistical as well as systematic uncertainties from the JES correction are shown for the total background and signal.

Selection	Background contributions				Total Background	Data	Signal	
	Multijet	$Z/\gamma^* \rightarrow ll$	$t\bar{t}$	Diboson			Point A	Point B
Preselection	304.5	286.7	12.4	28.6	$632.3 \pm 19.5^{+0.0}_{-0.0}$	596	$65.9 \pm 2.4^{+0.0}_{-0.0}$	$26.6 \pm 0.7^{+0.0}_{-0.0}$
Emu 1	194.4	115.4	10.4	25.3	$345.4 \pm 15.0^{+0.7}_{-0.7}$	329	$54.1 \pm 2.2^{+0.0}_{-0.0}$	$22.7 \pm 0.7^{+0.0}_{-0.0}$
Emu 2	8.6	20.0	9.1	21.2	$58.9 \pm 3.8^{+2.2}_{-2.2}$	52	$31.6 \pm 1.7^{+0.8}_{-0.0}$	$19.0 \pm 0.6^{+0.0}_{-0.1}$
Emu 3	5.9	3.6	7.4	20.2	$37.1 \pm 2.7^{+0.9}_{-0.9}$	34	$26.0 \pm 1.5^{+0.3}_{-0.0}$	$17.3 \pm 0.6^{+0.2}_{-0.2}$

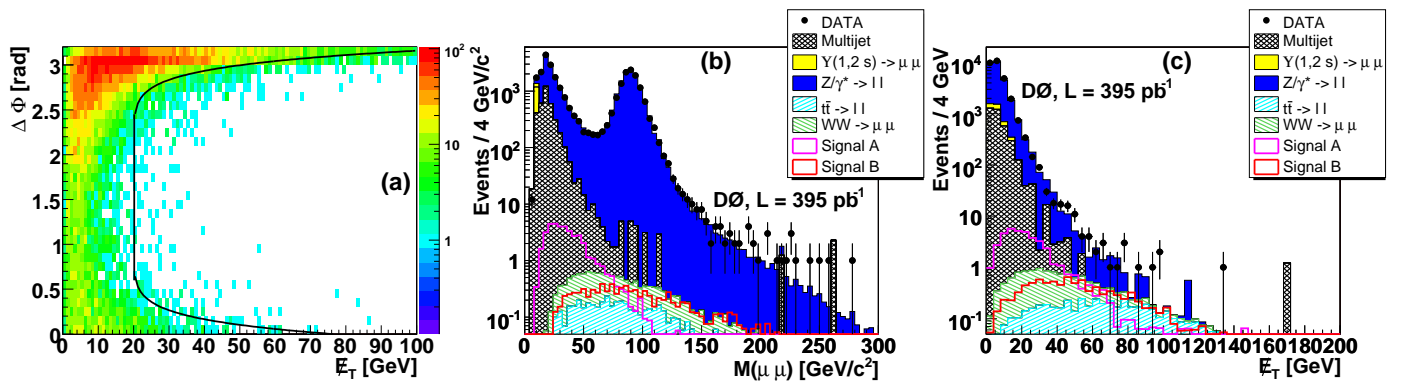


FIG. 2: $\mu\mu$ channel. (a) $\Delta\phi(\mu_1, \cancel{E}_T)$ versus \cancel{E}_T in simulated $Z/\gamma^* \rightarrow \mu\mu$ events; the contour of the cut Dimu 2 is shown by the black line. Distributions of the invariant mass of the two most energetic muons (b) and \cancel{E}_T (c) after preselection cuts (color available online).

TABLE II: $\mu\mu$ channel. Expected numbers of events in various background and signal channels, and number of observed events in data, at various selection levels. Statistical as well as systematic uncertainties from the JES correction are shown for the total background and signal.

Selection	Multijet	Background contributions				Total Background	Data	Signal	
		$\Upsilon(1S)$	$Z/\gamma^* \rightarrow \ell\ell$	$t\bar{t}$	WW			Point A	Point B
Preselection	3608	788	23782	5.1	9.6	$28377 \pm 348^{+0.0}_{-0.0}$	28733	$9.8 \pm 0.4^{+0.0}_{-0.0}$	$41.1 \pm 1.5^{+0.0}_{-0.0}$
Dimu 1	682	61	3895	5.1	1.5	$4664 \pm 97^{+452}_{-533}$	4337	$8.8 \pm 0.4^{+0.1}_{-0.1}$	$24.2 \pm 1.1^{+1.5}_{-1.9}$
Dimu 2	42	0	156	4.7	1.1	$203 \pm 8^{+52}_{-22}$	213	$7.5 \pm 0.3^{+0.2}_{-0.1}$	$12.9 \pm 0.8^{+1.2}_{-1.3}$
Dimu 3	0	0	6.1	2.6	0	$8.7 \pm 1.6^{+1.3}_{-0.1}$	4	$3.5 \pm 0.2^{+0.2}_{-0.0}$	$3.4 \pm 0.4^{+0.4}_{-0.3}$
Dimu 4	0	0	0.1	2.3	0	$2.9 \pm 0.4^{+0.1}_{-0.1}$	1	$3.1 \pm 0.2^{+0.2}_{-0.0}$	$3.3 \pm 0.4^{+0.4}_{-0.3}$

The expected numbers of background and signal events depends on several measurements and parametrizations which each introduce a systematic uncertainty: lepton identification and reconstruction efficiency [(2.6–7)%] [11], trigger efficiency [(3.5–5)%] [11], luminosity [6.1%] [13], multijet background modeling [10%], JES [(4–22)%] [15], jet identification and reconstruction efficiency and resolution [(4–16)%] [11], jet tagging [(1–11)%] [14], PDF uncertainty affecting the signal efficiency [10%].

After applying all selection cuts for $e\mu$ and $\mu\mu$ data sets, no evidence for \tilde{t}_1 production is observed. We combine the number of expected signal and background events and their corresponding uncertainty, and the number of observed events in data from the twelve bins of the $e\mu$ selection and the five bins of the $\mu\mu$ selection to calculate upper-limit cross sections for signal production at the 95% C.L. for various signal points using the modified frequentist approach [16]. In this calculation, correlated errors are taken into account; no overlap is expected nor observed between the two samples. Regions for which the calculated cross section upper limit is smaller than the theoretical one are excluded at 95% C.L. Figure 3 shows the excluded region as a function of the scalar top quark and sneutrino masses, for mean (continuous black line) and for both minimal and maximal (yellow band) values of the $\tilde{t}_1\bar{\tilde{t}}_1$ production cross section; the latter variation corresponds to the PDF uncertainty for the signal cross section, quadratically added to the $2\mu_r$ and $\mu_r/2$ renormalization scale variations of the $\tilde{t}_1\bar{\tilde{t}}_1$ cross section.

In summary, we have searched for the lightest scalar top quark decaying into $b\ell\tilde{\nu}$; events with an electron and a muon, and two muons have been considered for this search. No evidence for the lightest stop is observed in these decays, leading to a 95% C.L. exclusion in the $[M(\tilde{t}_1), M(\tilde{\nu})]$ plane. The largest stop mass excluded is 186 GeV/c^2 for a sneutrino mass of 71 GeV/c^2 , and the largest sneutrino mass excluded is 107 GeV/c^2 for a stop mass of 145 GeV/c^2 . This search extends the sensitivity of D0 well beyond the one reached in Run I [12].

We thank the staffs at Fermilab and collaborating institutions, and acknowledge support from the DOE and NSF (USA); CEA and CNRS/IN2P3 (France); FASI, Rosatom and RFBR (Russia); CAPES, CNPq, FAPERJ,

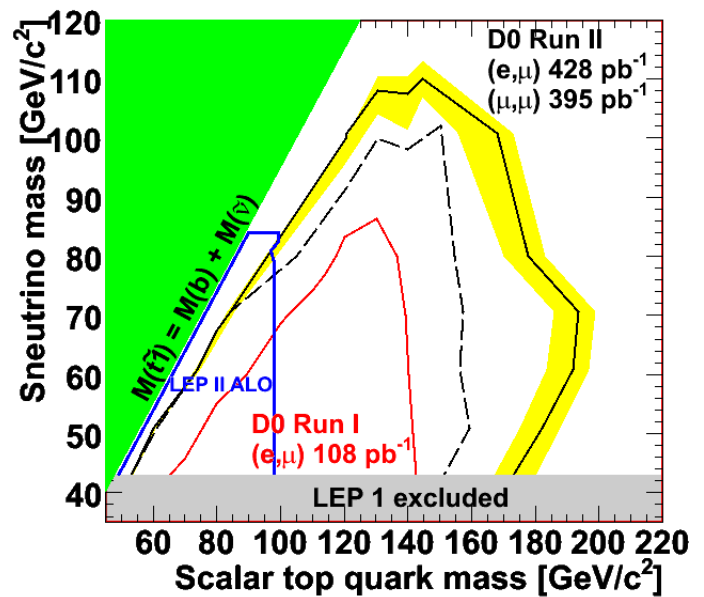


FIG. 3: 95% C.L. excluded region in the $[M(\tilde{t}_1), M(\tilde{\nu})]$ plane for the observed (continuous black line) and the average expected limits (discontinuous black line); the yellow band around the black line represents the lower and upper bounds of the signal cross-section variation. The excluded region for the observed limits of the D0 search during Run I [12] is also shown (red line). The blue line and green area respectively show the LEP II result [17], and the kinematic limit for $\tilde{t}_1 \rightarrow b\ell\tilde{\nu}$ decays (color available online).

FAPESP and FUNDUNESP (Brazil); DAE and DST (India); Colciencias (Colombia); CONACyT (Mexico); KRF and KOSEF (Korea); CONICET and UBACyT (Argentina); FOM (The Netherlands); Science and Technology Facilities Council (United Kingdom); MSMT and GACR (Czech Republic); CRC Program, CFI, NSERC and WestGrid Project (Canada); BMBF and DFG (Germany); SFI (Ireland); The Swedish Research Council (Sweden); CAS and CNSF (China); Alexander von Humboldt Foundation; and the Marie Curie Program.

-
- [1] S.P. Martin, in “Perspectives on Supersymmetry,” ed. G.L. Kane (World Scientific, Singapore 1998); revised version arXiv:hep-ph/9709356v4.
- [2] H. Hikasa and M. Kobayashi, *Phys. Rev. D* **36**, 724 (1987).
- [3] D0 Collaboration, V.M. Abazov *et al.*, *Phys. Lett. B* **645**, 119 (2007).
- [4] D0 Collaboration, V.M. Abazov *et al.*, *Nucl. Instrum. Methods A* **565**, 463 (2006).
- [5] A. Pukhov *et al.*, User’s manual for version 3.3, INP-MSU 98-41/542.
- [6] T. Sjöstrand *et al.*, *Comput. Phys. Commun.* **135**, 238 (2001).
- [7] M.L Mangano *et al.*, *JHEP* **0307**, 001 (2003).
- [8] H.L Lai *et al.*, *Eur. Phys. J.* **C12**, 375 (2000).
- [9] R. Brun and F. Carminati, CERN Program Library Long Writeup W5013, 1993 (unpublished).
- [10] G.C. Blazey *et al.*, in *Proceedings of the Workshop: QCD and Weak Boson Physics in Run II*, edited by U. Baur, R.K. Ellis, and D. Zeppenfeld, Fermilab-Pub-00/297 (2000).
- [11] D0 Collaboration, V.M. Abazov *et al.*, Fermilab-Pub-07/143E (2007).
- [12] D0 Collaboration, V.M. Abazov *et al.*, *Phys. Rev. Lett.* **88**, 171802 (2002).
- [13] T. Andeen *et al.*, Fermilab-TM-2365-E (2006).
- [14] S. Greder, Ph.D. thesis, Fermilab-Thesis-2004-28, 2004; B. Clément, Ph.D. thesis, Fermilab-Thesis-2006-06, 2006.
- [15] D0 Collaboration, V.M. Abazov *et al.*, *Phys. Rev. D* **75**, 092001 (2007).
- [16] T. Junk, *Nucl. Instrum. Methods A* **434**, 435 (1999).
- [17] LEP SUSY Working Group, ALEPH, DELPHI, L3, OPAL experiments, note LEPSUSYWG/04-02.1.